Available online at www.sciencedirect.com
SCIENCE DIRECT®

Spectrochimica Acta Part A 64 (2006) 216–232

SPECTROCHIMICA ACTA
PART A

www.elsevier.com/locate/saa

Synthesis and thermal characterization of new ternary chelates of piroxicam and tenoxicam with glycine and DL-phenylalanine and some transition metals

M.A. Zayed, F.A. Nour El-Dien, Gehad G. Mohamed*, Nadia E.A. El-Gamel

Chemistry Department, Faculty of Science, Cairo University, Giza, Egypt

Received 11 March 2005; received in revised form 7 June 2005; accepted 14 June 2005

Abstract

The ternary chelates of piroxicam (Pir) and tenoxicam (Ten) with Fe(II), Fe(III), Co(II), Ni(II), Cu(II) and Zn(II) in the presence of various amino acids such as glycine (Gly) or DL-phenylalanine (PhA) were prepared and characterized with different physicochemical methods. IR spectra confirm that Pir and Ten behave as a neutral bidentate ligand coordinated to the metal ions via the pyridine-*N* and carbonyl group of the amide moiety. Gly molecule acted as a uninegatively monodentate ligand and coordinate to the metal ions through its deprotonated carboxylic group. In addition, PhA acted as a uninegatively bidentate ligand and coordinate to the metal ions through its deprotonated carboxylic and amino groups. The solid reflectance spectra and magnetic moment measurements confirm that all the chelates have octahedral geometrical structures while Cu(II)- and Zn(II)-ternary chelates with PhA have square planar geometrical structures. Thermal behaviour of the complexes is extensively studied using TG and DTA techniques. TG results show that water molecules (hydrated and coordinated) and anions are removed in the first and second steps while Gly, PhA, Pir and Ten are decomposed in the next and subsequent steps. The pyrolyses of the chelates into different gases are observed in the DTA curves as exo- or endothermic peaks. Also, phase transition states are observed in some chelates. Different thermodynamic parameters are calculated using Coats–Redfern method and the results are interpreted.

Keywords: Piroxicam and tenoxicam ternary chelates; IR; Magnetic and diffuse reflectance spectra; Thermal analyses

1. Introduction

An intensive number of studies on the formation of mixed ligand complexes reveal a realization of their growing importance, particularly in their role in biological process [1]. The formation of mixed ligand chelates is a general feature of systems where a metal is present with two or more ligands. The study of these complexes shows that their formations are a favoured process over that of simple complexes [2]. The study of ternary complexes involving an aromatic amine as the primary ligand, various amino acids and biomolecules as secondary ligands can serve as useful models for gaining a better understanding of enzyme–metal ion–substrate complexes, which play an important role in metalloenzyme-catalysed biochemical reactions [3–5]. Rheumatoid arthritis is a disease characterized by painful disorders in the muscle and joints. At present, therapeutical treatment, for this illness are mainly based on non-steroidal anti-inflammatory drugs (NSAIDs), characterized by rapid and complete uptake in the blood stream and thus possessing a fast analgesic action [6]. Piroxicam (4-hydroxy-2-methyl-*N*-(2-pyridyl)-2H-1,2-benzothiazine-3-carboxamide 1,1-dioxide) and Tenoxicam (4-hydroxy-2-methyl-*N*-(2-pyridyl)-2H-thieno[2,3-e]-1,2-thiazine-3-carboxamide1,1-dioxide), are the most important members of oxicams class (Fig. 1) to be strong chelators for several divalent metal ions. Pir has been found to act as a monodentate ligand through pyridyl N with Pt(II) [7,8], a bidentate chelate ligand through its pyridyl N and amide O with Cd(II) and Cu(II) [6,9] and a tridentate ligand via the enolic oxygen, the amide nitrogen and pyridyl nitrogen with the organotin $[SnBu_2(Pir)]_n$, complex [10]. Tenoxicam

---

* Corresponding author.
E-mail address: ggenidy@hotmail.com (G.G. Mohamed).

1386-1425/$ – see front matter © 2005 Elsevier B.V. All rights reserved.
doi:10.1016/j.saa.2005.06.042

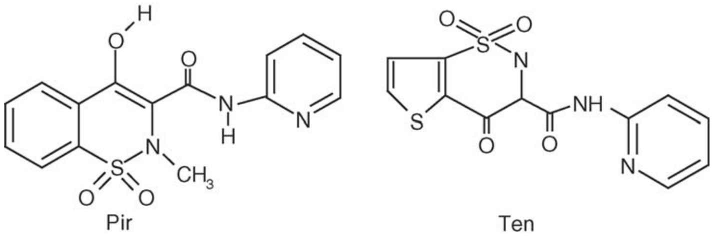

Fig. 1. Structural formula for piroxicam and tenoxicam.

forms complexes with first row transition metal ions, including Cu(II), Cu(Ten)$_2$·2H$_2$O [11]. Spectroscopic and magnetic properties suggested that Ten can act as a monoanionic ligand through the enolate oxygen and amide oxygen atom [11]. However, Ten forms a stable chelate with Cu(II) by employing the amide oxygen and pyridyl nitrogen of the drug molecule [12].

With the aim to continue the exploration of the coordination mode adopted by Pir and Ten, we have performed a preparative and structural work by using Pir and Ten (as primary ligands) with various amino acids (such as Gly and PhA) as secondary ligands with some ‘d-block’ metal ions. The amide oxygen and pyridyl nitrogen of the drug molecules with deprotonated carboxylate group in unidentate manner of Gly and uninegatively bidentate through deprotonated carboxylate and amino groups of PhA were employed. The solid chelates are characterized using different physico-chemical methods like elemental analyses (C, H, N, S and M), IR, magnetic moment and diffuse reflectance spectra. The thermal behaviour of the complexes (TG and DTA) are the main objective of this study in order to elucidate their thermal stability via following their mass loss with temperature as well as the changes accompanying these weight losses via DTA technique. Different thermodynamic parameters were calculated using Coats–Redfern method.

2. Experimental

2.1. Materials

All chemicals used were of the analytical reagent grade (AR), and of highest purity available. They included Pir (an authentic sample was kindly supplied by Pfizer Company, Cairo, Egypt) and Ten (sample was supplied by Eipico Company, Egypt) and their melting points was checked to confirm their purity. PhA was supplied from Acros, USA, while Gly was supplied from Sigma. Copper (II) acetate dihydrate (Prolabo); cobalt (II) and nickel (II) chlorides hexahydrate (BDH); zinc acetate dihydrate (Ubichem), anhydrous ferrous sulphate (Sigma) and ferric chloride hexahydrated (Prolabo). Zinc oxide, disodium salt of ethylenediaminetetraacetic acid, EDTA (Analar), ammonia solution (33%, v/v) and ammonium chloride (El-Nasr Pharm. Chem. Co., Egypt). Absolute ethyl alcohol, diethylether and nitric acid (Analar) were supplied from ADWIC. Hydrogen peroxide and sodium hydroxide were supplied from Prolabo. De-ionized water collected from all glass equipments was usually used in all preparations.

2.2. Instrumentation

Elemental microanalysis of the separated solid chelates for C, H, N and S were performed in the Microanalytical Center of Cairo University. Infrared spectra were recorded on a Perkin-Elmer FT-IR type 1650 spectrophotometer in wave number region 4000–200 cm^{-1}. The spectra were recorded as KBr pellets. The solid reflectance spectra were measured on a Shimadzu 3101PC spectrophotometer. The molar magnetic susceptibility was measured on powdered samples using the Faraday method. The diamagnetic corrections were made by Pascal’s constant and Hg[Co(SCN)$_4$] was used as calibrant. The thermogravimetric analysis (TGA and DTGA) and differential thermal analysis (DTA) were carried out in dynamic nitrogen atmosphere (20 mL min^{-1}) with a heating rate of 10 °C min^{-1} using Shimadzu TGA-50H and DTA-50H thermal analysers, respectively. Metal contents were determined by titration against standard EDTA after complete decomposition of the complexes with aqua regia in kjeldahl flask.

2.3. Synthesis

A hot ethanol solutions (60 °C) of the respective metal chlorides (Fe(II), Fe(III), Co(II) and Ni(II)) or acetate (Cu(II) and Zn(II)) (1 mmol) in de-ionized water (25 mL) were added to a mixture of 25 mL hot ethanol solution (60 °C) of Pir (0.331 g, 1 mmol) or Ten (0.337 g, 1 mmol) and 25 mL of 1 mmol Gly (0.075 g in de-ionized water) or 25 mL of 1 mmol PhA (0.165 g in ethanol) in the molar ratio 1:1:1 (metal salt:Pir or Ten:Gly or PhA) in total volume 75 mL mixture. The resulting mixture was stirred under reflux for 30 min. The complexes were precipitated as microcrystalline powders. They were removed by filtration, washed with hot ethanol followed by diethyl ether and dried in a vacuum desiccator over anhydrous calcium chloride.

3. Results and discussion

All the solid complexes are coloured products and separated as crystalline powder. The results of the elemental analyses of ternary chelates are listed in Tables 1 and 2. It was

Table 1
Analytical and physical data of piroxicam (Pir) and tenoxicam (Ten) ternary chelates with Gly

Compound	Chemical formula	Colour	mp (°C)	Found (calcd.) (%)					μ_{eff} (B.M.)	Λ_m (Ω^{-1} cm^2 mol^{-1})
				C	H	N	S	M		
Piroxicam [Pir]	$C_{15}H_{13}N_3O_4S$	White	198	54.50 (54.38)	3.70 (3.90)	12.34 (12.68)	9.55 (9.66)	–	–	–
Tenoxicam [Ten]	$C_{13}H_{11}N_3O_4S_2$	Yellow	210	46.35 (46.29)	3.55 (3.26)	12.20 (12.46)	19.25 (18.99)	–	–	–
[Gly]	$C_2H_5NO_2$	White	245 (dec)	32.00 (31.80)	6.80 (6.60)	18.42 (18.66)	–	–	–	–
Fe(II)–Pir–Gly	$[Fe(Pir)_2(Gly)_2]\cdot 4.5H_2O$	Reddish brown	193	42.90 (43.08)	4.35 (4.54)	11.70 (11.83)	6.32 (6.76)	5.67 (5.91)	5.12	17.70
Fe(III)–Pir–Gly	$[Fe(Pir)_2(Gly)_2]Cl\cdot 2H_2O$	Reddish brown	169	43.15 (43.52)	4.20 (4.05)	11.86 (11.95)	6.90 (6.82)	5.70 5.97	5.92	130
Co(II)–Pir–Gly	$[Co(Pir)_2(Gly)_2]\cdot 4H_2O$	Orange	204	43.65 (43.35)	3.45 (3.61)	11.85 (11.90)	6.75 (6.80)	5.66 (6.27)	5.10	29.0
Ni(II)–Pir–Gly	$[Ni(Pir)_2(Gly)_2]\cdot 4H_2O$	Light green	218	43.25 (43.35)	3.45 (3.60)	11.95 (11.90)	6.70 (6.80)	6.27 (6.27)	2.98	22.0
Cu(II)–Pir–Gly	$[Cu(Pir)_2(Gly)_2]\cdot 1.5H_2O$	Olive green	159	46.60 (46.23)	4.55 (4.19)	12.75 (12.69)	7.35 (7.25)	7.62 (7.19)	2.0	10.1
Zn(II)–Pir–Gly	$[Zn(Pir)_2(Gly)_2]\cdot 2H_2O$	Lemon	223	44.40 (44.31)	4.10 (4.17)	12.30 (12.29)	6.98 (7.02)	7.14 (7.28)	Diam	25.0
Fe(II)–Ten–Gly	$[Fe(Ten)_2(Gly)_2]\cdot 5H_2O$	Reddish brown	189	37.10 (37.19)	4.00 (4.13)	11.35 (11.57)	13.42 (13.22)	5.52 (5.78)	4.95	26.8
Fe(III)–Ten–Gly	$[Fe(Ten)_2(Gly)_2]Cl\cdot H_2O$	Reddish brown	125	38.83 (38.62)	3.50 (3.43)	11.87 (12.02)	13.34 (13.48)	5.76 (6.01)	5.60	120
Co(II)–Ten–Gly	$[Co(Ten)_2(Gly)_2]\cdot 3.5H_2O$	Orange	186	38.40 (38.14)	4.10 (3.92)	11.75 (11.86)	13.52 (13.56)	6.51 (6.25)	4.70	24.0
Ni(II)–Ten–Gly	$[Ni(Ten)_2(Gly)_2]\cdot 3.5H_2O$	Light green	161	38.25 (38.14)	3.95 (3.92)	11.81 (11.86)	13.61 (13.56)	6.81 (6.25)	3.15	20.0
Cu(II)–Ten–Gly	$[Cu(Ten)_2(Gly)_2]\cdot H_2O$	Olive green	201	40.05 (39.82)	3.55 (3.32)	12.41 (12.39)	14.50 (14.16)	7.55 (7.02)	1.95	9.3
Zn(II)–Ten–Gly	$[Zn(Ten)_2(Gly)_2]\cdot 2.5H_2O$	Lemon	203	38.90 (38.63)	3.80 (3.76)	12.16 (12.02)	13.50 (13.73)	6.80 (6.98)	Diam	15.3

Table 2
Analytical and physical data of piroxicam (Pir) and tenoxicam (Ten) ternary chelates with PhA

Compound	Chemical formula	Colour	mp (°C)	Found (calcd.) (%)					μ_{eff} (B.M.)	Λ_m (Ω^{1} cm^2 mol^{-1})
				C	H	N	S	M		
[PhA]	$C_9H_{11}NO_2$	White	267 (dec)	65.60	6.43 (65.45)	8.60 (6.6)	– (8.48)	– (8.48)	–	–
Fe(II)–Pir–PhA	$[Fe(Pir)(PhA)(H_2O)_2]0\cdot 5SO_4$	Reddish brown	200	45.50 (45.35)	4.21 (4.25)	8.60 (8.82)	7.72 (7.56)	8.29 (8.82)	4.91	156
Fe(III)–Pir–PhA	$[Fe(Pir)(PhA)Cl_2]\cdot H_2O$	Reddish brown	218	44.95 (45.00)	3.90 (4.06)	8.70 (8.75)	4.90 (5.00)	4.52 (4.38)	5.70	15.70
Co(II)–Pir–PhA	$[Co(Pir)(PhA)(H_2O)_2]Cl$	Orange	140	46.12 (46.06)	4.45 (4.30)	8.85 (8.95)	5.40 (5.12)	9.60 (9.43)	5.40	115
Ni(II)–Pir–PhA	$[Ni(Pir)(PhA)(H_2O)_2]Cl$	Light green	175	46.25 (46.04)	4.48 (4.30)	8.87 (8.95)	5.25 (5.11)	9.27 (9.43)	3.40	105
Cu(II)–Pir–PhA	$[Cu(Pir)(PhA)](Ac)\cdot H_2O$	Olive green	170	46.20 (49.09)	4.45 (4.40)	8.75 (8.81)	5.25 (5.03)	9.36 (9.99)	1.70	120
Zn(II)–Pir–PhA	$[Zn(Pir)(PhA)(H_2O)_2](Ac)\cdot H_2O$	Lemon	220	46.40 (46.36)	4.80 (4.90)	8.44 (8.32)	4.60 (4.75)	9.32 (9.66)	Diam	135
Fe(II)–Ten–PhA	$[Fe(Ten)(PhA)(H_2O)_2]0.5SO_4\cdot 1.5H_2O$	Reddish brown	203	39.40 (39.50)	4.09 (4.20)	8.35 (8.38)	11.78 (11.97)	8.52 (8.38)	5.20	174
Fe(III)–Ten–PhA	$[Fe(Ten)(PhA)Cl_2]\cdot H_2O$	Reddish brown	145	40.83 (40.87)	3.55 (3.40)	8.70 (8.67)	9.80 (9.91)	8.96 (9.67)	5.40	9.0
Co(II)–Ten–PhA	$[Co(Ten)(PhA)(H_2O)_2]Cl\cdot 2H_2O$	Orange	195	39.50 (39.55)	4.15 (4.30)	8.50 (8.39)	9.42 (9.58)	8.58 (8.84)	4.20	120
Ni(II)–Ten–PhA	$[Ni(Ten)(PhA)(H_2O)_2]Cl$	Light green	180	41.63 (41.80)	3.69 (3.96)	8.72 (8.87)	10.18 (10.13)	9.30 (9.34)	2.86	90
Cu(II)–Ten–PhA	$[Cu(Ten)(PhA)](Ac)\cdot 2.5H_2O$	Olive green	200	43.45 (43.31)	4.60 (4.48)	8.55 (8.37)	9.40 (9.57)	9.41 (9.49)	1.78	110
Zn(II)–Ten–PhA	$[Zn(Ten)(PhA)\cdot(H_2O)_2](Ac)\cdot H_2O$	Lemon	200	42.20 (42.41)	4.72 (4.56)	8.26 (8.25)	9.10 (9.43)	9.59 (9.57)	Diam	142

seen from Table 1 that ternary chelates of di- and tri-valent transition metals with Pir or Ten and Gly are formed with 1:2:2 ratio (metal salts:Pir or Ten:Gly). The chelates have the general formula $[M(H_2L)_2(Gly)_2]\cdot yH_2O$, where M = Fe(II), Co(II), Ni(II), Cu(II) and Zn(II) and $y = 1$–5; while Fe(III) ternary chelates have the formula $[Fe(H_2L)_2(Gly)_2]Cl\cdot yH_2O$, $y = 1$–2. The mixed ligand complexes of Pir or Ten and PhA (Table 2) with the same transition metals are formed with 1:1:1 ratio [metal salts:Pir or Ten:PhA]. The Fe(II), Co(II), Ni(II), Cu(II) and Zn(II) ternary chelates have the formula $[M(H_2L)(PhA)\cdot(H_2O)_z](x)\cdot yH_2O$, where x = acetate in case of Cu(II) ($z = 0$) and Zn(II) ($z = 2$); sulphate in case of Fe(II) ($z = 2$) or Cl in case of Co(II) ($z = 2$) and Ni(II) ($z = 2$) and $y = 1$–2.5. Whereas in case of Fe(III) ternary chelates, it have the formula $[Fe(H_2L)(PhA)(Cl)_2]\cdot H_2O$.

3.1. IR spectra and mode of bonding

The careful inspection of the of the IR spectra of free Pir or Ten and their ternary complexes, was made in order to facilitate the assignment of these bands in the free ligand and its metal chelates. The strong bands observed at 1630 and 1636 cm^{-1} in the free Pir and Ten, respectively, are assigned to the stretching vibration of the C=O group. In Pir and Ten complexes, these bands are shifted to lower frequencies (3–36 cm^{-1}) or disappear supporting the participation of the carbonyl group in the coordination [13]. The bands located at 1572 and 1599 cm^{-1} are assigned to the ν(C=N) stretching vibration of pyridyl nitrogen of Pir and Ten, respectively. These bands disappeared but it is still difficult to confirm their participation in chelate formation as they overlapped with those of the carboxylate group of the amino acids or the amide II stretching vibration band. Its participation is confirmed from the band due to in-plane deformation ρ(py) located at 624 cm^{-1}. After complexation, this band disappeared and a new band at 630–669 cm^{-1} is found in the ternary chelates [14].

Two bands, located at 1351–1330 and 1041–1040 cm^{-1}, are assigned to the asymmetric and symmetric stretching vibrations of the SO_2 group, respectively. These two SO_2 bands are shifted to lower or higher frequencies in accordance to the assignment of Cini et al. [9]. As the SO_2 group is not involved in metal binding, this shift to higher frequencies must be related to important hydrogen bonding effects [15,16]. The bands at the wave number 1594–1586 and 1412–1408 cm^{-1} regions, in the free amino acids; Gly or PhA, are assigned to the asymmetric and symmetric stretching vibrations of the carboxylate group, respectively. The shift of these two bands to higher or lower frequencies suggest the participation of –COOH group in complex formation after deprotonation [17,18]. In the 3500–3000 cm^{-1} IR region of the ternary chelates of Pir and Ten, the overlap of the various ν(NH) vibrations coupled in many cases with molecules of water of hydration gives rise to very strong absorption. This prevents the individual recognition of the various bands. The band due to the in-plane deformation of the amino group of Gly (δNH_2) at 1524 cm^{-1} is slightly shifted to higher or lower frequencies (1516–1528 cm^{-1}) upon chelation indicating non-participation of the nitrogen atom in bonding to the metal ions [18]. The shift to higher or lower wave numbers may be attributed to the participation of the NH_2 group in intermolecular hydrogen bond. While the band due to δNH_2 of DL-phenylalanine is assigned to a maximum near 1502 cm^{-1} is red shifted to the extent 10–23 cm^{-1} in all the complexes confirming coordination of the NH_2 group to the metal ions [19,20].

The ν(M–N) bands of the pyridyl nitrogen are appeared in the wave number range 566–590 cm^{-1} for the divalent and at 523–597 cm^{-1} for the trivalent metal ion[137]. While the ν(M–N) bands [21] of the PhA ternary chelates are observed in the region 313–432 cm^{-1}. New peaks of weak or medium intensity are observed in the wave number range 297–386 cm^{-1} which are attributed to ν(M–O) vibrations of ternary chelates [22]. The stretching vibration bands due to ν(M–O) of amino acids (Gly and PhA) appeared in the region of 313–54 cm^{-1}, as reported for $[Cu(Gly)_2]$ and $[Cu(ala)_2]$ complexes [21,23]. The band at 334–45 cm^{-1} is assigned to the M–Cl vibration of Fe(III) ternary complexes with Pir or Ten and PhA [24]. The vibrations of the sulphate ion in Fe(II) ternary chelates with PhA appear at 1160–1147 and 630–629 cm^{-1}. These indicate the uncoordinated nature of sulphate group [25].

3.2. Magnetic susceptibility and electronic spectra measurements

The diffuse reflectance spectra of the Fe(III)-chelates exhibit a band at 21,930–21,140 cm^{-1}, which may be assigned to the $^6A_{1g} \to T_{2g}$ (G) transition in octahedral geometry of the complexes [26]. The observed magnetic moment values are 5.1–5.92 B.M. which confirm the octahedral geometry in Fe(III) ion [27]. The diffused reflectance spectra of the mixed ligand complexes of Fe(II) ion display two absorption bands at 12,200–11,630 and 22,220–17,730 cm^{-1} which are assigned to $^5T_{2g} \to {}^5Eg$ transition and charge transfer, respectively [28]. The Fe(II)-ternary chelates exhibit magnetic moment values of 4.91–5.80 B.M., which are consistent with a high spin octahedral geometry [29].

The Ni(II)-mixed ligand complexes have magnetic moment values of 2.86–3.40 B.M.; which are in the normal range observed for octahedral Ni(II)-complexes [30]. Their electronic spectra display three bands, in the solid reflectance spectra at ν_1, 12,630–11,610 cm^{-1}; $^3A_{2g} \to {}^3T_{2g}$, ν_2, 15,770–14,640 cm^{-1}; $^3A_{2g} \to {}^3T_{1g}$ (F) and ν_3, 20,280–19,080 cm^{-1}; $^3A_{2g} \to {}^3T_{1g}$ (P). The 10 Dq values lie in the 11,610–12,630 cm^{-1} ranges, again confirming the octahedral configuration of the chelates [31]. The electronic spectra of the ternary Co(II) complexes give three bands at 12,270–11,310, 15,040–13,890 and 17,590–16,340 cm^{-1} wave number regions, respectively. The third region 18,180–26,060 cm^{-1} refers to the charge transfer band. The bands observed are assigned to the transitions $^4T_{1g}$ (F) → $^4T_{2g}$ (F) (ν_1), $^4T_{1g}$ (F) → $^4A_{2g}$ (F) (ν_2) and $^4T_{1g}$ (F) → $^4T_{2g}$ (P) (ν_3), respectively, suggesting that there is an octahedral geometry around Co(II) ion [32]. The magnetic susceptibility measurements lie in the 4.2–5.4 B.M. range which is an indicative of octahedral geometry [33].

The reflectance spectra of Cu(II) ternary chelates in the presence of Gly (as second ligand) consist of a broad, low intensity shoulder centered at (17,860–16,340 cm^{-1}) that forms part of the charge transfer band. The magnetic moment of 1.95–2.0 B.M. falls within the range normally observed for octahedral Cu(II) complexes [34]. While, the Cu(II)–ternary chelates in the presence of PhA (as second ligand) exhibit a broad band in the region 16,670–15,380 cm^{-1} assigned to $^2E_g \rightarrow {}^2T_{2g}$ transition and broad band in the region 14,710–14,160 cm^{-1} which is assigned to $^2B_{1g} \rightarrow {}^2A_{1g}$ as well as a shoulder band in the range 17,540–17,610 cm^{-1} characteristic of a square planner geometry for Cu(II) complexes [35]. The magnetic moments of the Cu(II)-complexes are found to be 1.7–1.83 B.M.

In analogy with those described for Zn(II) complexes containing N–O donor Schiff bases [36] and according to the empirical formulae of these complexes, we proposed an octahedral geometry for the mixed ligand Zn(II) complexes of Pir and Ten (as primary ligands) and Gly or PhA (as secondary ligands) with two axial position occupied by the two glycine molecules or water molecules in case of Pir or Ten mixed ligand complexes with PhA.

3.3. Thermal analyses (TGA and DTA)

The TGA, DTG and DTA curves of the ternary chelates are shown in Figs. 2–5 and the results are listed in Tables 3–6. Thermal analyses of ternary chelates elicit the following points to the light.

The thermograms of Fe(II)-ternary chelates, namely **1**, **7**, **13** and **19**, show three decomposition steps within the temperature range 25–830 °C (Figs. 2a–5a). The first step of decomposition, within the temperature range 25–200 °C, corresponds to the loss of hydrated water molecules with a mass loss of 8.91% (calcd. for $4.5H_2O$; 8.55%), 8.96% (calcd. for $5H_2O$; 9.29%), 8.0% (calcd. for $0.5SO_4{}^{2-}$; 7.56%) and 8.15% (calcd. for $0.5SO_4{}^{2-}$ and $0.5H_2O$; 8.53%) for **1**, **7**, **13** and **19** chelates, respectively. The DTA curves, illustrated in Figs. 2a–5a, show that this dehydration step is endothermic process for chelates **1** and **7**, while for chelates **13** and **19**, an exo- and endothermic peaks are appeared as the result of dehydration and sulphate elimination. The second and third steps in the temperature range 185–830 °C; correspond to the elimination of coordinated water, Pir, Ten, Gly^- and PhA^- molecules leaving metal disulphide (in case of **1** and **7** chelates) or metal oxide (in case of **13** and **19** chelates) as a residue. The overall weight loss amounts to 87.86% (calcd. 87.33%), 88.17% (calcd. 87.61%), 89.33% (calcd. 88.66%) and 89.40% (calcd. 89.23%) for **1**, **7**, **13** and **19** chelates, respectively. The elimination of coordinated water, Pir, Ten, Gly^- and PhA^- molecules as different fragments is accompanied by the appearance of several endo- and exothermic peaks in the DTA curves as illustrated in Figs. 2–5. The DTA curve of chelate 19 shows an endothermic peak at 1118 °C, which may be attributed to a phase transition.

The thermograms of Fe(III) chelates; **8**, **14**, **20**, show three decomposition steps within the temperature range 25–890 °C. Whereas Fe(III) chelate; **2**, show four decomposition steps within the temperature range 25–700 °C. The first step of decomposition within the temperature range 25–165 °C corresponds to the loss of water molecules of hydration with a mass loss of 3.61% (calcd. for $2H_2O$; 3.84%), 1.27% (calcd. for H_2O; 1.93%), 3.35% (calcd. for H_2O; 2.81%) and 2.25% (calcd. for H_2O; 2.78%) for **2**, **8**, **14** and **20** chelates, respectively. The DTA curves (Figs. 2b–5b and Tables 3–6) show that this dehydration step gives endothermic and/or endo- and exothermic peaks within the temperature of decomposition. The second, third and fourth steps (from 120 to 890 °C) correspond to the removal of Cl_2, Gly^-, PhA^-, Pir and Ten molecules leaving metal oxide or sulphide as a residue. The overall weight loss amounts to 83.71% (calcd. 82.93%), 87.65% (calcd. 87.12%), 83.20% (calcd. 83.75%) and 86.06% (calcd. 86.38%) for **2**, **8**, **14** and **20** chelates, respectively. The decomposition of Pir, Ten, Gly^-, PhA^- and Cl_2 molecules is accompanied by the appearance of several exo- and endothermic peaks as shown in the DTA curves (Figs. 2b–5b and Tables 3–6). Also, phase transitions are observed in the DTA curves for the chelates **2**, **14** and **20**.

The Co(II) complexes; **3**, **9**, **15** and **21**, exhibit three to four steps of decomposition as given by TGA analyses (Figs. 2c–5c). The first decomposition step (within the temperature range 25–195 °C) corresponds to the loss of $4H_2O$ (mass loss 7.87%; calcd. 7.65%), $3.5H_2O$ (mass loss 6.65%; calcd. 6.67%), $(1/2)Cl_2$ (mass loss 5.22%; calcd. 5.68%), and $(1/2)Cl_2$ and H_2O (mass loss 7.64%; calcd. 8.01%) for **3**, **9**, **15** and **21** chelates, respectively. The exo- and endothermic peaks have been observed in the DTA curves (Figs. 2c–5c) within the temperature range of this dehydration step. The loss of coordinated water, Pir, Ten, Gly^- and PhA molecules takes place within the temperature range 140–960 °C with mass losses of 84.94% (calcd. 84.38%), 85.07% (calcd. 84.41%), 83.17% (calcd. 82.33%) and 81.60% (calcd. 80.76%) for **3**, **9**, **15** and **21** chelates, respectively. According to the DTA curves, given in Figs. 2c–5c, these decomposition steps give several exo- and endothermic peaks as the result of elimination of the ligand molecules to different fragments.

The TGA curves of the Ni(II)-ternary chelates, namely **4**, **10**, **16** and **22**, show three to four stages of decomposition within the temperature range of 25–750 °C. The first stage at 25–210 °C corresponds to the loss of water molecules of hydration and $(1/2)Cl_2$ gas, while the second, third and fourth stages involve the loss of Pir, Ten, Gly^-, PhA^- and coordinated water molecules. The overall weight loss amounts to 92.03% (calcd. 92.03%), 91.34% (calcd. 92.06%), 88.63%

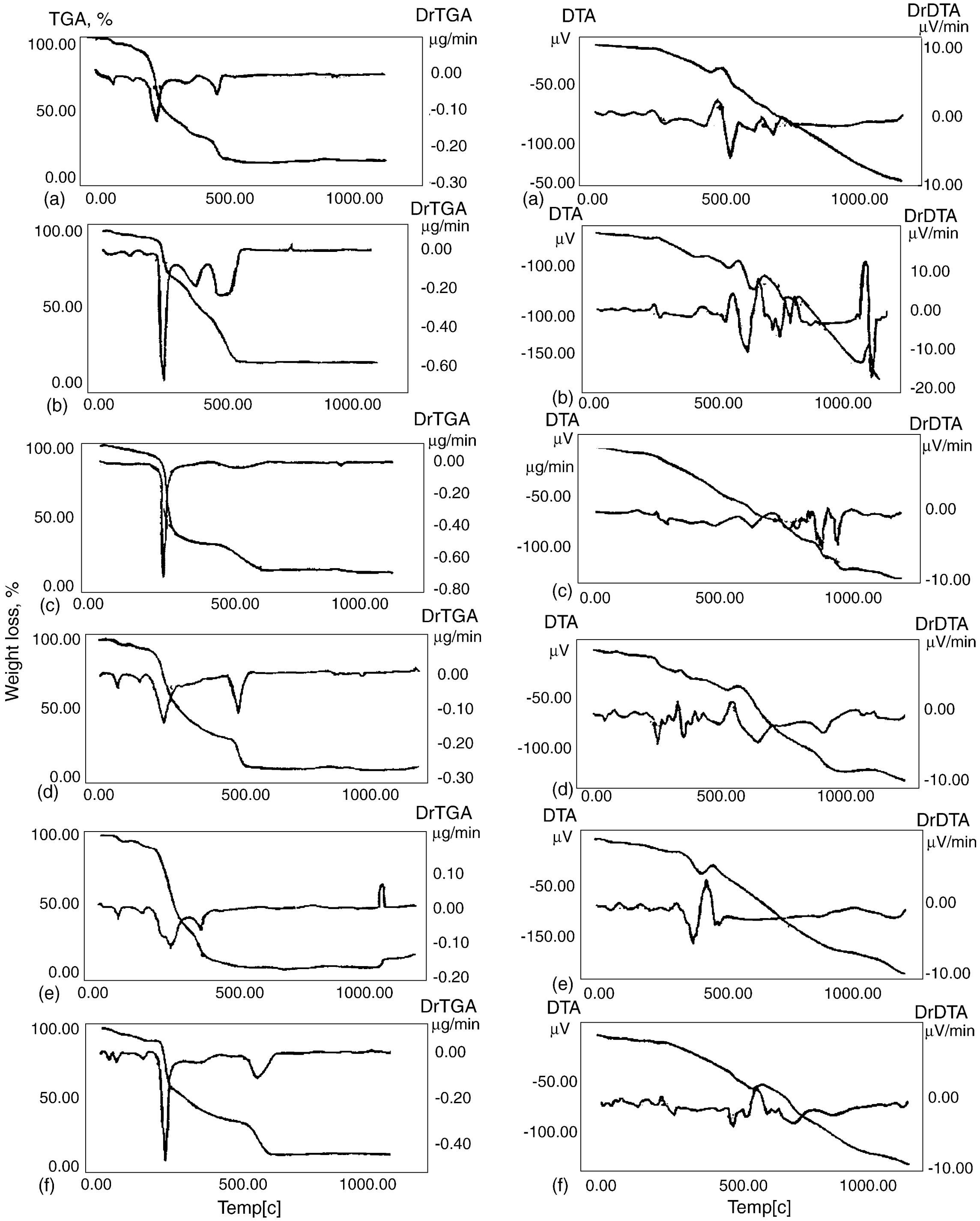

Fig. 2. Thermal analyses (TG and DTA) of Pir and Gly mixed ligand chelates: (a) Fe(II), (b) Fe(III), (c) Co(II), (d) Ni(II), (e) Cu(II) and (f) Zn(II).

(calcd. 88.01%) and 85.65% (calcd. 85.59%) for **4**, **10**, **16** and **22** chelates, respectively. The DTA curves of these chelates are illustrated in Figs. 2d–5d and the results are listed in Tables 3–6. The chemical changes accompanying the elimination of water, anion, and ligand molecules is observed as exo- or endothermic peaks in the DTA curves.

On the other hand the Cu(II) chelates; **5**, **11**, **17** and **23**, exhibit three decomposition steps (Figs. 2e–5e). The first step in the temperature range 30–155 °C (mass loss = 2.96%; calcd. for $1.5H_2O$; 3.06%), 25–90 °C (mass loss = 2.46%; calcd. for H_2O; 1.99%), 25–170 °C (mass loss = 2.64%; calcd. for H_2O; 2.83%) and 45–200 °C (mass loss = 6.27%; calcd. for $2.5H_2O$; 6.73%) may accounted for the loss of water molecules of hydration for **5**, **11**, **17** and **23** chelates, respectively. As shown in Tables 3–6, the mass losses of the remaining decomposition steps amount to 90.47% (calcd.

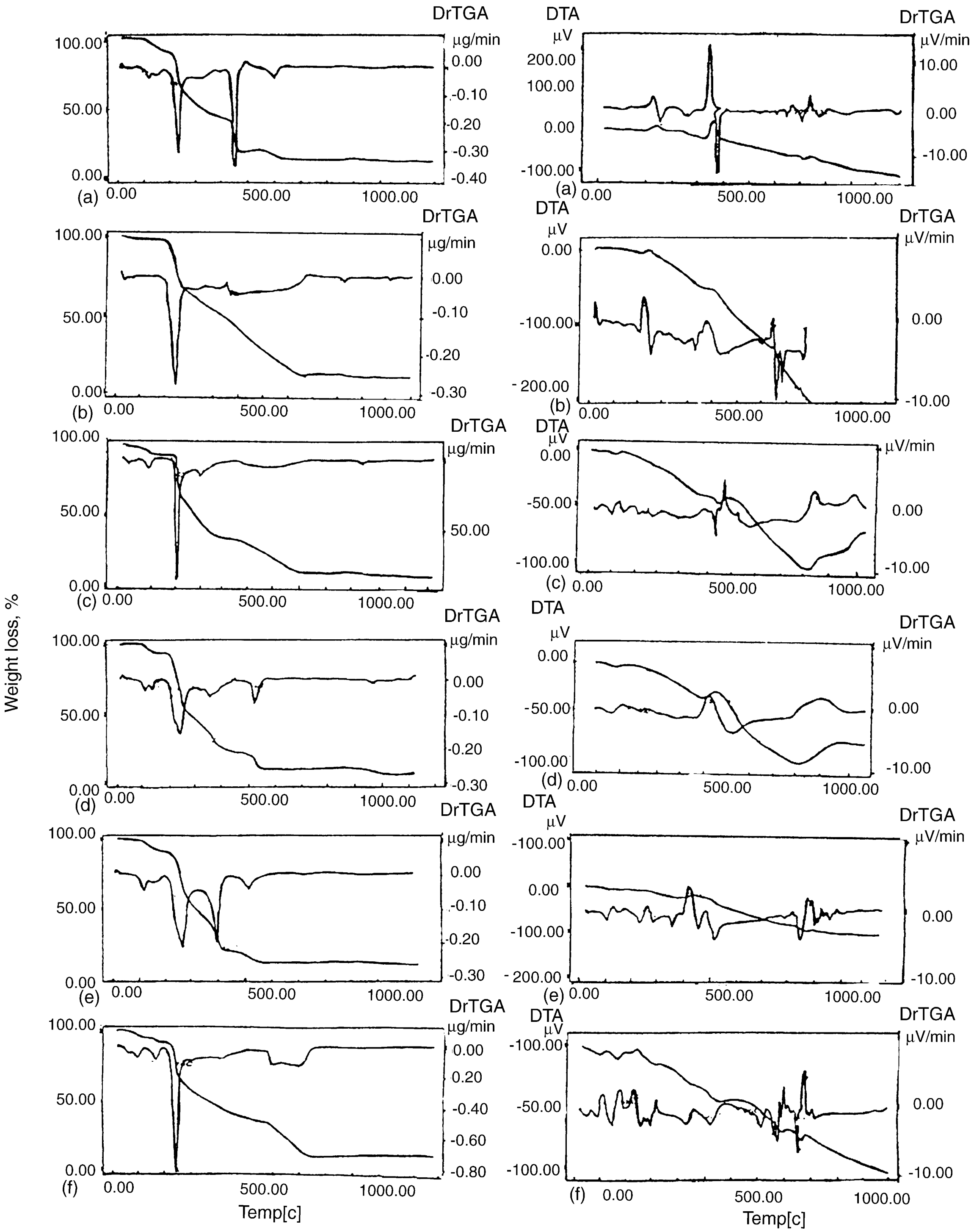

Fig. 3. Thermal analyses (TG and DTA) of Ten and Gly mixed ligand chelates: (a) Fe(II), (b) Fe(III), (c) Co(II), (d) Ni(II), (e) Cu(II) and (f) Zn(II).

91.00%), 90.54% (calcd. 91.21%), 88.28% (calcd. 87.49%) and 88.23% (calcd. 88.11%) for **5**, **11**, **17** and **23**, respectively. They correspond to the removal of Pir, Ten, Gly$^-$, PhA$^-$ and Ac$^-$ molecules leaving CuO as a residue.

The TGA curves of the Zn-ternary chelates, **6**, **12**, **18** and **24**, represent three decomposition steps as illustrated in Figs. 2f–5f and Tables 3–6. The first step of decomposition within the temperature range (25–220 °C) correspond to the loss of hydrated water molecules with a mass loss of 4.62% (calcd. for $2H_2O$; 3.95%), 4.87% (calcd. for $2.5H_2O$; 4.83%), 8.81% (calcd. for $3H_2O$; 8.02%) and 8.44% (calcd. for $3H_2O$; 7.95%) for **6**, **12**, **18** and **24**, respectively. The DTA curves show that, this dehydration step is appeared as endothermic and/or endo- and exothermic peaks. The remaining steps of

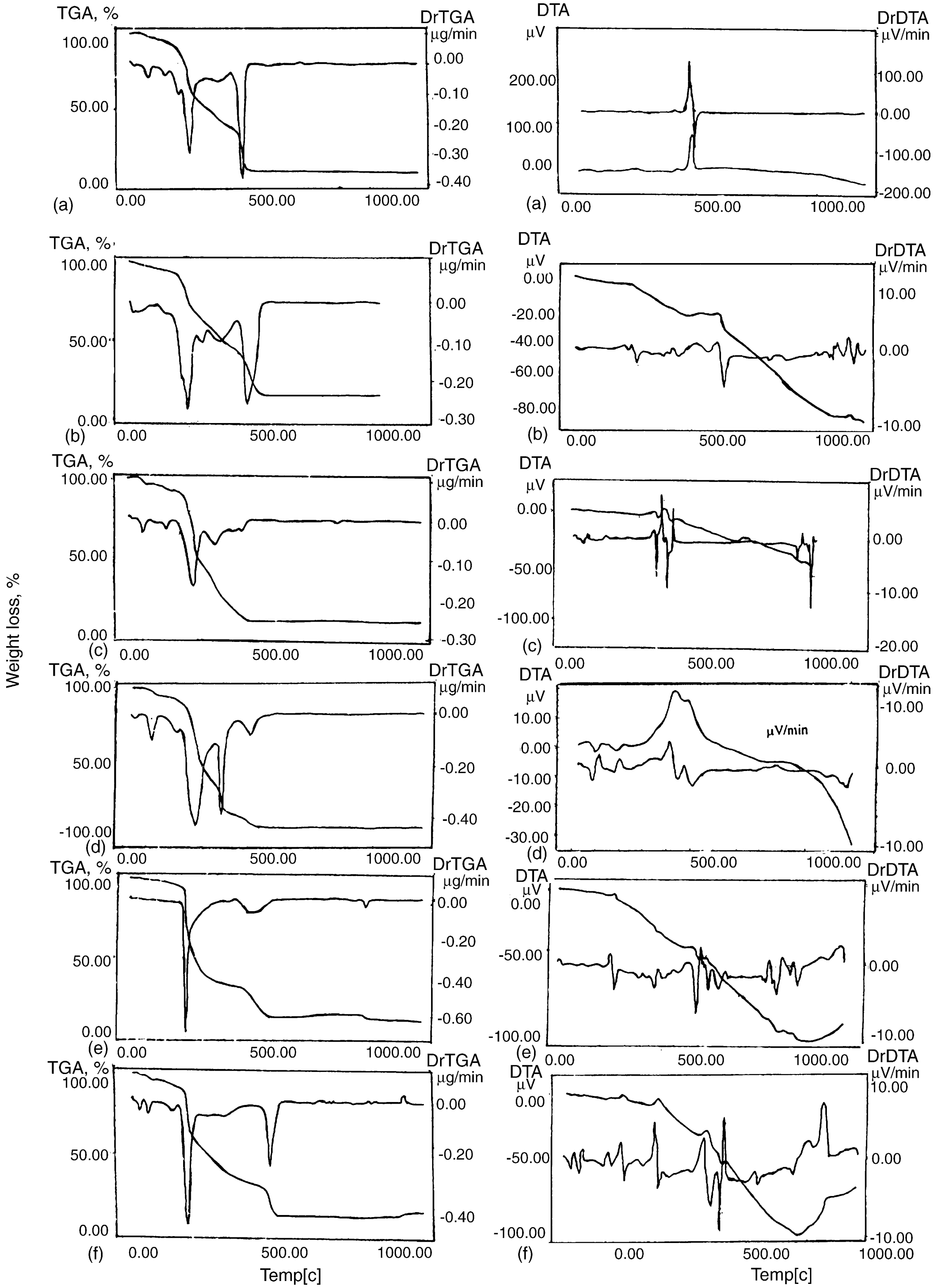

Fig. 4. Thermal analyses (TG and DTA) of Pir and PhA mixed ligand chelates: (a) Fe(II), (b) Fe(III), (c) Co(II), (d) Ni(II), (e) Cu(II) and (f) Zn(II).

decomposition within the temperature range 110–1100 °C correspond to the removal of these ligands as gases and this is accompanied by the appearance of exo- and endothermic peaks in the DTA curves and the position of these exo- and endothermic peaks is given in Tables 3–6. The overall weight loss amounts to 89.35% (calcd. 89.14%), 89.51% (calcd. 89.59%), 88.38% (calcd. 87.96%) and 88.05% (calcd. 88.07%) for chelates **6**, **12**, **18** and **24** chelates, respectively.

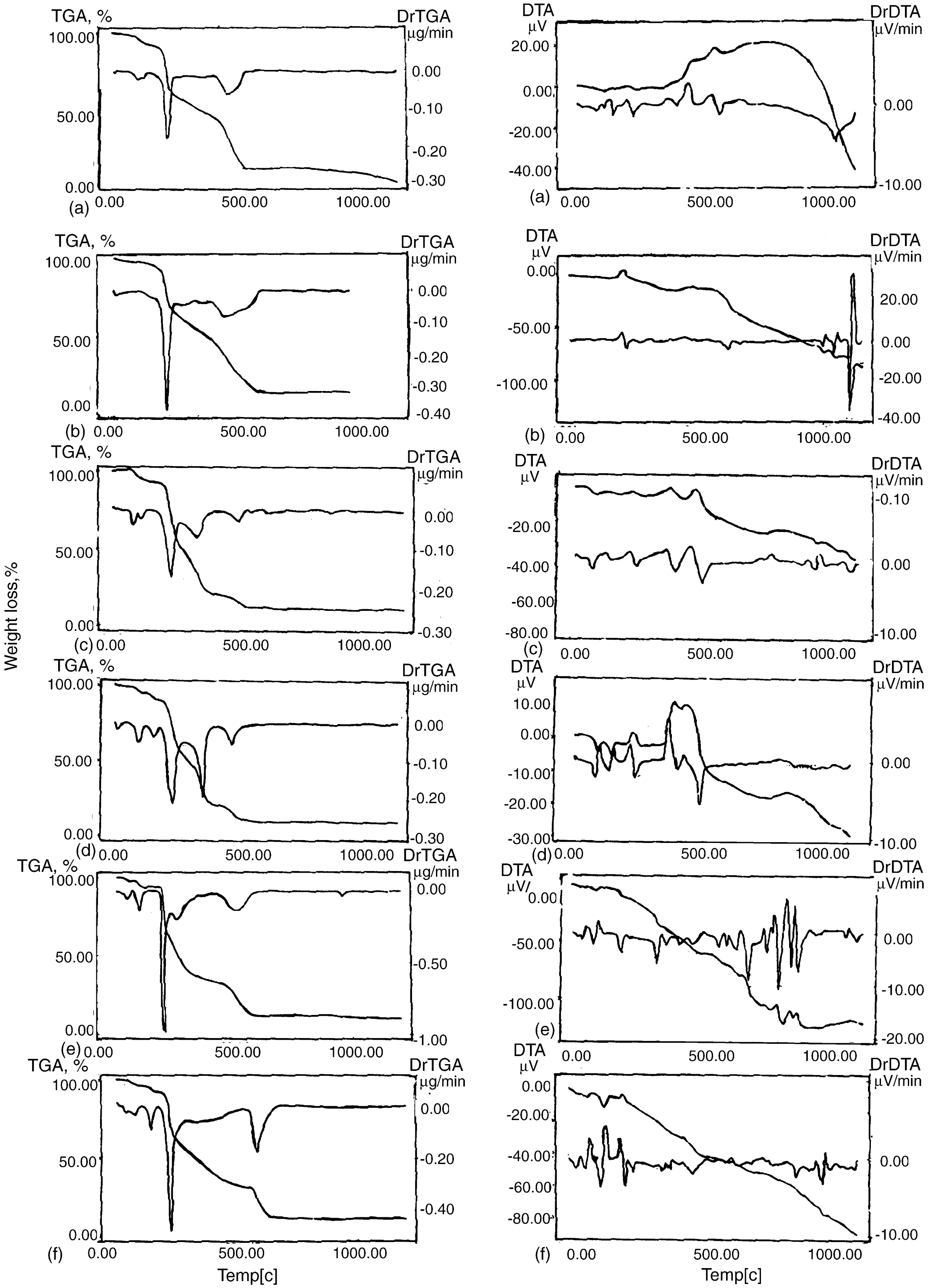

Fig. 5. Thermal analyses (TG and DTA) of Ten and PhA mixed ligand chelates: (a) Fe(II), (b) Fe(III), (c) Co(II), (d) Ni(II), (e) Cu(II) and (f) Zn(II).

Table 3
Thermoanalytical data of Pir–Gly ternary chelates

Complex	Temperature range (°C)	Peak temperature in DTA (°C)	No. of decomposition steps	% Found (calcd.)		Assignment	Metallic residue
				Mass loss	Total mass loss		
[**1**]	25–200	63(+), 130(+), 190(+)	1.0		8.91 (8.55)	Loss of 4.5H_2O	FeS_2
	200–656	284(+), 430(+), 476(−), 508(+), 621(−), 654(+), 686(−)	2.0	78.95 (78.78)	87.86 (87.33)	Loss of Pir and Gly molecules	
[**2**]	25–165	105(+), 136(−)	1.0		3.61 (3.84)	Loss of 2H_2O	Fe_2O_3
	165–680	200(−), 250(−), 282(+), 454(−), 530(+), 573(−), 620(+), 673(−)	3.0	80.10 (79.09)	83.71 (82.93)	Loss of (1/2)Cl_2, Pir and Gly molecules	
		732(+), 766(+), 790(−), 820(−), 885(+), 1110(−), 1135(+)				Phase transition	
[**3**]	25–195	66(+), 105(−), 143(+), 200(+)	1.0		7.87 (7.65)	Loss of 4H_2O	CoO
	195–960	268(+), 310(−), 343(−), 365(+), 400(−), 430(−), 541(−), 640(+), 883(+)	2.0	84.94 (84.38)	92.81 (92.03)	Loss of Pir and Gly molecules	
		1040(+), 1070(−), 1177(+)				Phase transition	
[**4**]	25–210	77(+), 107(−), 150(+), 190(−)	1.0		8.20 (7.65)	Loss of 4H_2O	NiO
	210–600	270(−), 320(−), 391(+), 440(−), 488(+)	2.0	84.01 (84.38)	92.03 (92.03)	Loss of Pir and Gly molecules	
		880(+), 958(+), 1154(+)				Phase transition	
[**5**]	30–155	40(+), 80(+)	1.0		2.96 (3.06)	Loss of 1.5H_2O	CuO
	155–1225	181(−), 250(−), 297(+), 398(+), 482(+), 620(+), 699(−), 780(−), 840(−), 880(+), 920(−), 950(+), 1163(+)	2.0	87.51 (87.94)	90.47 (91.00)	Loss of Pir and Gly molecules	
[**6**]	25–110	50(+), 85(+), 110(+)	1.0		4.62 (3.95)	Loss of 2H_2O	ZnS
	110–710	156(+), 200(−), 245(−), 290(+), 370(+), 499(+), 550(+), 584(−), 630(+), 670(+), 722(+), 798(−), 864(+), 1128(+)	2.0	84.73 (85.19)	89.35 (89.14)	Loss of Pir and Gly molecules	

(+) = Endothermic, (−) = exothermic, [**1**] = $[Fe(II)(Pir)_2(Gly)_2]\cdot 4.5H_2O$, [**2**] = $[Fe(III)(Pir)_2(Gly)_2]Cl\cdot 2H_2O$, [**3**] = $[Co(II)(Pir)_2(Gly)_2]\cdot 4H_2O$, [**4**] = $[Ni(II)(Pir)_2(Gly)_2]\cdot 4H_2O$, [**5**] = $[Cu(II)(Pir)_2(Gly)_2]\cdot 1.5H_2O$, [**6**] = $[Zn(II)(Pir)_2(Gly)_2]\cdot 2H_2O$.

Table 4
Thermoanalytical data of Ten–Gly ternary chelates

Complex	Temperature range (°C)	Peak temperature in DTA (°C)	No. of decomposition steps	% Found (calcd.)		Assignment	Metallic residue
				Mass loss	Total mass loss		
[7]	25–185	105(+)	1.0		8.96 (9.29)	Loss of $5H_2O$	FeS_2
	185–830	220(−), 256(+), 363(+), 445(−), 480(+), 749(+), 778(−), 840(−), 810(+), 870(+), 974(+)	2.0	79.48 (78.32)	88.17 (87.61)	Loss of Ten and Gly molecules	
[8]	25–125	30(+), 100(+)	1.0		1.27 (1.93)	Loss of H_2O	FeS_2
	125–890	150(+), 225(−), 255(+), 320(+), 431(+), 470(−), 700(+), 741(−), 758(+), 782(+), 865(+)	2.0	86.38 (85.19)	87.65 (87.12)	Loss of (1/2)Cl_2, Ten and Gly molecules	
[9]	25–180	100(+), 144(−)	1.0		6.65 (6.67)	Loss of $3.5H_2O$	CoO
	180–710	626(+), 519(−)	3.0	85.07 (85.41)	91.72 (92.08)	Loss of Ten and Gly molecules	
		860(+), 1111(−)				Phase transition	
[10]	25–160	107(+), 130(−)	1.0		6.49 (6.67)	Loss of $3.5H_2O$	NiO
	160–750	174(−), 261(−), 290(+), 355(+), 390(−), 417(−), 455(+), 517(+), 842(+), 870(−), 930(+), 977(−)	3.0	84.85 (85.39)	91.34 (92.06)	Loss of Ten and Gly molecules	
[11]	25–90	50(+), 101(+)	1.0		2.46 (1.99)	Loss of H_2O	CuO
	90–840	137(−), 210(+), 250(−), 281(+), 400(+), 570(−), 536(+), 674(+), 860(+)	2.0	88.08 (89.22)	90.54 (91.21)	Loss of Ten and Gly molecules	
		946(−), 1104(−), 1020(+)				Phase transition	
[12]	25–130	60(+), 95(+), 114(−)	1.0		4.87 (4.83)	Loss of $2.5H_2O$	ZnS
	130–800	147(+), 163(−), 232(−), 250(+), 290(+), 300(+), 310(−), 410(+), 459(−), 573(−), 714(+), 790(−), 770(+)	2.0	84.64 (84.76)	89.51 (89.59)	Loss of Ten and Gly molecules	
		851(+), 876(−), 915(−), 1176(+)				Phase transition	

(+) = Endothermic, (−) = exothermic, [**7**] = $[Fe(II)(Ten)_2(Gly)_2]\cdot 5H_2O$, [**8**] = $[Fe(III)(Ten)_2(Gly)_2]Cl\cdot H_2O$, [**9**] = $[Co(II)(Ten)_2(Gly)_2]\cdot 3.5H_2O$, [**10**] = $[Ni(II)(Ten)_2(Gly)_2]\cdot 3.5H_2O$, [**11**] = $[Cu(II)(Ten)_2(Gly)_2]\cdot H_2O$, [**12**] = $[Zn(II)(Ten)_2(Gly)_2]\cdot 2.5H_2O$.

Table 5
Thermoanalytical data of Pir–PhA ternary chelates

Complex	Temperature range (°C)	Peak temperature in DTA (°C)	No. of decomposition steps	% Found (calcd.)		Assignment	Metallic residue
				Mass loss	Total mass loss		
[**13**]	30–200	120(−)	1.0	81.33 (81.10)	8.00 (7.56)	Loss of $0.5SO_4^{2-}$	FeO
	200–560	480(−), 490(+)	2.0		89.33 (88.66)	Loss of $2H_2O$, Pir and PhA molecules	
[**14**]	30–115	35(+)	1.0	79.85 (80.94)	3.35 (2.81)	Loss of H_2O	Fe_2S_3
	120–710	240(+), 275(+), 385(+), 450(+), 521(+), 631(+)	2.0		83.20 (83.75)	Loss of Cl_2, Pir and PhA molecules	
		812(+), 1071(+), 1091(−), 1136(+)				Phase transition	
[**15**]	25–140	95(+), 102(−)	1.0	83.17 (82.33)	5.22 (5.68)	Loss of $(1/2)Cl_2$	CoO
	140–605	430(+), 455(−), 484(+), 510(−)	2.0		88.39 (88.01)	Loss of $2H_2O$, Pir and PhA molecules	
		1111(+), 1130(−), 1179(+)				Phase transition	
[**16**]	30–170	95(+), 116(−)	1.0	83.14 (82.34)	5.49 (5.67)	Loss of $(1/2)Cl_2$	NiO
	170–700	205(−), 411(−), 470(+), 510(+)	3.0		88.63 (88.01)	Loss of $2H_2O$, Pir and PhA molecules	
		878(−), 1095(+), 1183(+)				Phase transition	
[**17**]	25–170	120(+)	1.0	85.64 (84.66)	2.64 (2.83)	Loss of H_2O	CuO
	170–681	190(−), 200(+), 251(+), 355(+), 380(+), 414(+), 450(+), 520(+), 594(+), 602(−), 638(+), 683(+)	2.0		88.28 (87.49)	Loss of acetate, Pir and PhA molecules	
		888(−), 922(+), 975(+), 1008(+), 1120(+)				Phase transition	
[**18**]	30–220	51(+), 85(+), 201(−)	1.0	79.57 (79.94)	8.81 (8.02)	Loss of $3H_2O$	ZnO
	220–762	250(−), 268(+), 320(−), 388(−), 403(+), 583(+), 615(+), 650(+), 665(−)	2.0		88.38 (87.96)	Loss of acetate, Pir and PhA molecules	
		790(+), 945(+), 1000(−), 1062(−)				Phase transition	

(+) = Endothermic, (−) = exothermic, [**13**] = $[Fe(II)(Pir)(PhA)(H_2O)_2]\cdot 0.5SO_4$, [**14**] = $[Fe(III)(Pir)(PhA)Cl_2]\cdot H_2O$, [**15**] = $[Co(II)(Pir)(PhA)(H_2O)_2]Cl$, [**16**] = $[Ni(II)(Pir)(PhA)(H_2O)_2]$ Cl, [**17**] = $[Cu(II)(Pir)(PhA)](Ac)\cdot H_2O$, [**18**] = $[Zn(II)(Pir)(PhA)(H_2O)_2](Ac)\cdot H_2O$.

Table 6
Thermoanalytical data of Ten–PhA ternary chelates

Complex	Temperature range (°C)	Peak temperature in DTA (°C)	No. of decomposition steps	% Found (calcd.)		Assignment	Metallic residue
				Mass loss	Total mass loss		
[**19**]	25–200	102(+), 140(+), 163(−)	1.0		8.15 (8.53)	Loss of $0.5SO_4^{2-}$ and $0.5H_2O$	FeO
	200–650	230(−), 259(+), 493(−), 600(−), 626(+)	2.0	81.25 (80.70)	89.40 (89.23)	Loss of $3H_2O$, Ten and PhA molecules	
		1118(+)				Phase transition	
[**20**]	30–140	–	1.0		2.25 (2.78)	Loss of H_2O	FeS
	140–715	236(−), 253(+), 510(+), 666(+)	2.0	83.81 (83.60)	86.06 (86.38)	Loss of Cl_2, Ten and PhA molecules	
		1040(−), 1051(+), 1071(−), 1098(+) 1144(−), 1160(+)				Phase transition	
[**21**]	45–190	94(+), 150(+)	1.0		7.64 (8.01)	Loss of $(1/2)Cl_2$ and H_2O	CoO
	190–810	283(+), 440(+), 555(+), 847.5(−)	3.0	81.60 (80.76)	89.24 (88.77)	Loss of $3H_2O$, Ten and PhA molecules	
		1020(+), 1040(−), 1130(+), 1178(+)				Phase transition	
[**22**]	25–160	102(+), 131(−)	1.0		5.92 (5.62)	Loss of $(1/2)Cl_2$	NiS
	160–640	170(+), 200(−), 270(−), 283(+), 426(−), 450(+), 555(+)	3.0	79.73 (79.97)	85.65 (85.59)	Loss of $2H_2O$, Ten and PhA molecules	
[**23**]	45–200	98(−), 138(−)	1.0		6.27 (6.73)	Loss of $2.5H_2O$	CuO
	200–830	229(+), 374(+), 420(+), 467(+), 520(+), 622(+), 670(+), 740(+), 740(+), 820(+)	2.0	81.96 (81.38)	88.23 (88.11)	Loss of acetate, Ten and PhA molecules	
		863(+), 896(+), 943(+), 1178(+)				Phase transition	
[**24**]	30–200	70(+), 92(+), 109(−), 152(+), 174(−)	1.0		8.44 (7.95)	Loss of $3H_2O$	
	200–870	220(−), 249(+), 270(+), 400(+), 526(+), 690(−)	2.0	79.61 (80.12)	88.05 (88.07)	Loss of acetate, Ten and PhA molecules	ZnO
		952(+), 1057(+), 1097(+)				Phase transition	

(+) = Endothermic, (−) = exothermic, [**19**] = $[Fe(II)(Ten)(PhA)(H_2O)_2]\cdot 0.5SO_4\cdot 1.5H_2O$, [**20**] = $[Fe(III)(Ten)(PhA)Cl_2]\cdot H_2O$, [**21**] = $[Co(II)(Ten)(PhA)(H_2O)_2]Cl\cdot 2H_2O$, [**22**] = $[Ni(II)(Ten)(PhA)(H_2O)_2]Cl$, [**23**] = $[Cu(II)(Ten)(PhA)](Ac)\cdot 2.5H_2O$, [**24**] = $[Zn(II)(Ten)(PhA)(H_2O)_2](Ac)\cdot H_2O$.

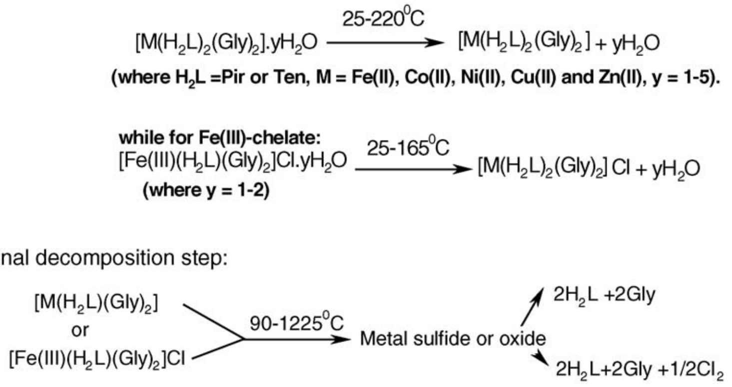

Scheme 1. Thermal decomposition of Pir and Ten ternary chelates with Gly.

Accordingly, the thermal decomposition of Pir or Ten in ternary chelates in the presence of Gly can be summarized as shown in Scheme 1.

For Pir or Ten ternary chelates with PhA, the thermal decomposition is shown in Scheme 2.

3.4. Kinetic study

The thermodynamic activation parameters of decomposition processes of dehydrated complexes namely activation energy (E^*), enthalpy (ΔH^*), entropy (ΔS^*) and Gibbs free energy change of the decomposition (ΔG^*) were evaluated graphically by employing the Coast–Redfern relation [37]:

$$\log\left[\frac{\log(W_{\mathrm{f}}/W_{\mathrm{f}}-W)}{T^2}\right] = \log\left[\frac{AR}{\theta E^*}\left(\frac{1-2RT}{E^*}\right)\right] - \frac{E^*}{2.303RT} \qquad (1)$$

where W_{f} is the mass loss at the completion of the reaction, W the mass loss up to temperature T; R the gas constant, E^* the activation energy in kJ mol^{-1}, θ the heating rate and $(1-(2RT/E^*)) \cong 1$. A plot of the left-hand side of Eq. (1) against $1/T$ gives a slope from which E^* was calculated and A (Arrhenius factor) was determined from the intercept. The entropy of activation (ΔS^*), enthalpy of activation (ΔH^*) and the free energy change of activation (ΔG^*) were calculated using the following equations:

$$\Delta S^* = 2.303\left(\frac{\log Ah}{KT}\right)R \qquad (2)$$

$$\Delta H^* = E^* - RT \qquad (3)$$

$$\Delta G^* = H^* - TS^* \qquad (4)$$

where K and h are the Boltzman and Planck constants, respectively. The calculated values of E^*, A, ΔS^*, ΔH^* and ΔG^* for the decomposition steps are given in Tables 7 and 8.

The activation energy for the elimination of water molecules of hydration or hydrated water from the Fe(II)-ternary chelates is shown in the range 64–174 kJ mol^{-1} (Tables 7 and 8). Regarding the Fe(III)-chelates, the activation energy of the first step is shown in the range 35–77 kJ mol^{-1}. Meanwhile, the data listed in Tables 7 and 8 show that the Co(II)- and Ni(II)-chelates are found to have activation energy for the elimination of water molecules of hydration in the range 8–108.3 and 60.55–137 kJ mol^{-1} for the Co(II) and Ni(II) chelates, respectively. Moreover, the Cu(II)- and Zn(II)-chelates exhibit an activation energy in the range 36.21–62.10 and 59.4–76.26 kJ mol^{-1} for the elimination of water molecules of hydration for the Cu(II)- and Zn(II)-chelates, respectively. From the acti-

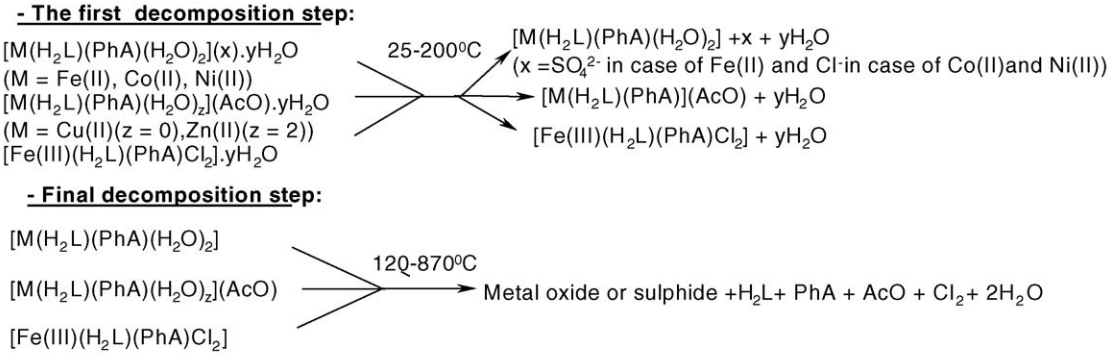

Scheme 2. Thermal decomposition of Pir and Ten ternary chelates with PhA.

Table 7
Kinetic data of the thermal decomposition of Pir–Gly and Ten–Gly mixed ligands

Complex	Decomposition range (°C)	E^* (kJ mol^{-1})	A (S^{-1})	ΔS^* (J K^{-1} mol^{-1})	ΔH^* (kJ mol^{-1})	ΔG^* kJ mol^{-1}
$[Fe(II)(Pir)_2(Gly)_2]\cdot 4.5H_2O$	25–200	128.4	1.20×10^{12}	−0.41	127.7	127.7
	200–326	130.5	2.50×10^{12}	−0.69	128.5	128.7
	326–656	224.8	9.37×10^{14}	−4.58	220.9	218.8
$[Fe(III)(Pir)_2(Gly)_2]Cl\cdot 2H_2O$	25–165	21.65	7.68×10^{2}	−32.87	20.95	22.97
	165–324	175.9	1.53×10^{16}	−7.92	173.7	171.6
	324–440	127.4	1.50×10^{9}	−8.59	124.2	127.5
	445–680	192.4	9.21×10^{11}	−2.43	188.3	189.5
$[Co(II)(Pir)_2(Gly)_2]\cdot 4H_2O$	25–195	99.7	5.37×10^{28}	−37.94	98.94	195.7
	195–355	106.6	1.72×10^{8}	−10.37	104.5	97.11
	355–960	169.2	3.25×10^{16}	−7.97	264.7	260.5
$[Ni(II)(Pir)_2(Gly)_2]\cdot 4H_2O$	25–210	137.0	1.45×10^{6}	−14.04	136.3	137.5
	210–367	112.0	3.02×10^{9}	−7.61	109.9	112.1
	367–600	259.6	3.18×10^{11}	−3.24	156.4	157.6
$[Cu(II)(Pir)_2(Gly)_2]\cdot 1.5H_2O$	30–155	48.90	2.68×10^{5}	−16.11	47.80	49.85
	155–380	22.99	7.44×10^{3}	−27.38	20.71	28.22
	380–1225	134.7	1.51×10^{6}	−15.87	130.1	138.9
$[Zn(II)(Pir)_2(Gly)_2]\cdot 2H_2O$	25–110	76.26	4.81×10^{10}	−32.00	75.75	75.95
	110–350	191.6	5.28×10^{17}	−11.47	189.4	186.4
	350–710	25.85	5.01×10^{6}	−3.22	210.9	212.8
$[Fe(II)(Ten)_2(Gly)_2]\cdot 5H_2O$	25–185	64.40	1.58×10^{7}	−12.10	63.28	64.91
	185–502	173.8	1.07×10^{17}	−9.96	171.8	169.4
	510–830	286.7	4.34×10^{19}	−15.34	282.9	276.0
$[Fe(III)(Ten)_2(Gly)_2Cl]\cdot H_2O$	25–125	35.14	4.74×10^{4}	−16.97	34.69	35.60
	125–341	151.4	3.63×10^{14}	−4.28	149.4	148.4
	341–890	63.61	2.6×10^{7}	−13.09	58.67	66.44
$[Co(II)(Ten)_2(Gly)_2]\cdot 3.5H_2O$	25–180	8.67	7.88×10^{9}	−5.75	79.69	80.36
	180–300	105.6	5.80×10^{9}	−6.72	103.7	105.2
	300–473	90.63	1.80×10^{6}	−15.24	87.64	93.12
	475–710	132.4	8.16×10^{20}	−18.11	128.0	318.4
$[Ni(II)(Ten)_2(Gly)_2]\cdot 3.5H_2O$	25–160	60.55	5.39×10^{6}	−13.14	59.46	61.18
	160–343	125.5	1.62×10^{11}	−3.51	123.4	124.3
	347–460	159.0	3.25×10^{11}	−3.23	155.8	157.0
	460–750	171.8	1.57×10^{10}	−6.54	167.6	171.0
$[Cu(II)(Ten)_2(Gly)_2]\cdot H_2O$	25–90	62.10	4.29×10^{17}	−10.93	61.13	62.40
	90–200	196.8	6.98×10^{18}	−14.14	194.8	191.4
	200–840	89.70	9.39×10^{5}	−16.41	87.71	94.49
$[Zn(II)(Ten)_2(Gly)_2]\cdot 2.5H_2O$	25–130	62.46	1.89×10^{8}	−9.16	61.75	62.54
	130–200	270.7	8.17×10^{26}	−32.71	268.7	260.7
	200–800	182.8	1.29×10^{9}	−9.29	177.3	183.4

vation energy values, one can conclude that, the water and anion molecules are easy to be eliminated from the ternary chelates according to the following order: Fe(II)-chelates > Ni(II)-chelates > Co(II)-chelates > Fe(III)-chelates > Zn(II)-chelates > Cu(II)-chelates.

According to the kinetic data obtained from DTG curves, all the complexes have negative entropy, which indicates that activated complexes have more ordered systems than reactants. From Tables 7 and 8, it is obvious that, the nickel complex shows a higher thermal stability than those of copper. This can be discussed in terms of repulsion among electron pairs in the valence shell of the central ion. The higher electronegativity of copper compared to that of nickel leads to a higher repulsion between bonding pairs in the valence shell of copper ion giving lower stability [32,38,39].

The lower thermal stability of the cobalt complex may be attributed to the higher repulsion between the multiple-bonding electron pairs (six bonds) in the valence shell of cobalt, as well as to the higher repulsion obtained by the non-bonded pairs of electrons on the axial donating oxygen of the water molecule and the bonded electrons [40].

3.5. Structural interpretation of ternary chelates

The structure of the ternary chelates of Pir or Ten and amino acids (Gly or PhA) with some di- and tri-valent tran-

Table 8
Kinetic data of the thermal decomposition of Pir–PhA and Ten–PhA mixed ligands

Complex	Decomposition range (°C)	E^* (kJ mol^{-1})	A (S^{-1})	ΔS^* (J K^{-1} mol^{-1})	ΔH^* (kJ mol^{-1})	ΔG^* (kJ mol^{-1})
$[Fe(II)(Pir)(PhA)(H_2O)_2]\cdot 0.5SO_4$	30–200	77.22	1.17×10^9	−7.76	76.49	77.14
	200–311	174.2	4.8×10^{16}	−9.15	172.1	169.9
	315–560	194.5	7.56×10^{11}	−2.67	190.2	191.5
$[Fe(III)(Pir)(PhA)Cl_2]\cdot H_2O$	32–115	35.54	3.71×10^4	−17.20	35.10	36.03
	120–468	107.1	6.05×10^9	−6.74	105.1	106.7
	468–710	238.3	1.04×10^{15}	−4.58	233.9	231.6
$[Co(II)(Pir)(PhA)(H_2O)_2]Cl$	25–140	106.0	7.85×10^{14}	−6.14	105.3	104.8
	140–325	156.9	9.24×10^{13}	−2.78	154.6	153.9
	325–605	160.0	6.82×10^{11}	−2.44	156.9	157.8
$[Ni(II)(Pir)(PhA)(H_2O)_2]Cl$	30–170	111.9	2.34×10^{14}	−4.62	110.9	110.5
	170–356	108.5	1.4×10^9	−8.35	106.1	108.5
	356–453	363.7	6.77×10^{27}	−34.36	360.5	347.2
	460–700	306.6	6.71×10^{19}	−15.67	302.4	294.5
$[Cu(II)(Pir)(PhA)](Ac)\cdot H_2O$	25–170	36.21	1.09×10^4	−18.75	35.62	36.97
	170–421	36.21	2.18×10^2	−23.93	34.09	40.19
	424–681	211.9	6.40×10^{12}	−0.533	207.6	207.9
$[Zn(II)(Pir)(PhA)(H_2O)_2](Ac)\cdot H_2O$	30–220	71.09	6.26×10^9	−5.62	70.40	70.87
	220–518	86.99	3.16×10^7	−12.05	84.84	87.95
	518–762	385.0	1.25×10^{16}	−6.93	380.3	376.2
$[Fe(II)(Ten)(PhA)(H_2O)_2]\cdot 0.5S\ O_4\cdot 1.5H_2O$	25–200	77.22	1.17×10^9	−7.76	76.49	77.14
	203–311	174.2	4.8×10^{16}	−9.15	172.1	169.9
	315–650	194.5	7.56×10^{11}	−2.67	190.2	191.5
$[Fe(III)(Ten)(PhA)Cl_2]\cdot H_2O$	30–137	43.70	1.02×10^6	−14.07	43.16	44.05
	140–372	192.8	5.07×10^{18}	−13.81	190.7	187.4
	372–712	108.1	6.48×10^5	−16.64	103.8	112.4
$[Co(II)(Ten)(PhA)(H_2O)_2]Cl\cdot 2H_2O$	45–190	108.3	2.31×10^{13}	−2.20	107.2	106.9
	190–332	216.3	3.85×10^{20}	−18.10	214.2	209.6
	332–490	58.44	2.55×10^{11}	−3.40	55.40	56.65
	495–810	223.3	1.51×10^{20}	−16.43	318.8	310.1
$[Ni(II)(Ten)(PhA)(H_2O)_2]Cl$	25–160	94.75	4.58×10^{11}	−1.72	93.74	93.95
	160–340	112.1	7.41×10^9	−6.61	109.9	111.7
	341–468	185.3	4.65×10^{13}	−1.74	182.0	181.4
	473–635	243.9	1.34×10^{15}	−4.82	239.6	237.2
$[Cu(II)(Ten)(PhA)](Ac)\cdot 2.5H_2O$	45–200	59.40	1.18×10^7	−12.10	58.56	59.80
	200–409	200.9	3.1×10^{29}	−38.61	298.7	289.0
	409–830	207.5	255×10^{12}	−1.48	203.9	203.1
$[Zn(II)(Ten)(PhA)(H_2O)_2](Ac)\cdot H_2O$	30–200	59.40	6.08×10^7	−10.25	58.72	59.56
	200–343	294.5	2.81×10^{29}	−38.55	292.5	283.0
	348–870	275.5	1.88×10^{15}	−5.00	270.5	267.5

sition metal ions (Fe(II), Fe(III), Co(II), Ni(II), Cu(II) and Zn(II)) were confirmed by the IR, magnetic, solid reflectance and thermal analyses data. For all the chelates, the chelation is brought by the pyridine nitrogen and C=O of amide groups of Pir or Ten or by the carboxylate and/or the amino groups of amino acids (Gly or PhA). The valence of the metal ions in the chelates is neutralized by the displacement of carboxylate proton of amino acids in case of ternary chelates. This is supported by the IR data. IR and thermal analyses confirmed the existence of water molecules of hydration and/or coordination. From the reflectance spectra and magnetic moment measurements, the geometrical structure of the ternary chelates were proposed and found to be octahedral,

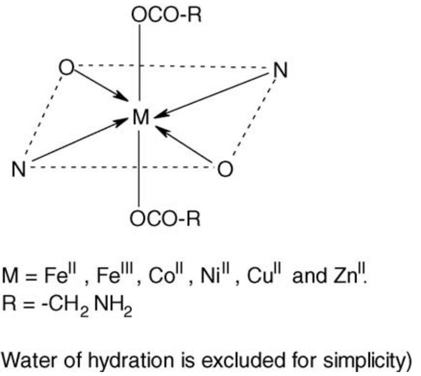

M = Fe^{II} , Fe^{III}, Co^{II} , Ni^{II} , Cu^{II} and Zn^{II}.
R = $-CH_2NH_2$

(Water of hydration is excluded for simplicity)

Fig. 6. Suggested structure of Pir or Ten ternary chelates with Gly.

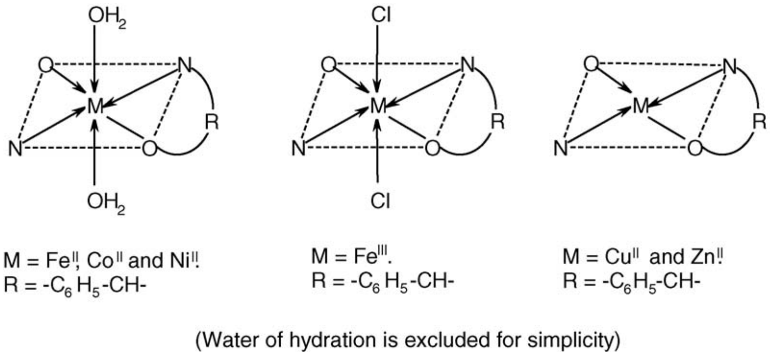

Fig. 7. Suggested structure of Pir or Ten ternary chelates with PhA.

tetrahedral or square planar. As a general conclusion, Pir or Ten behaves as neutral bidentate ligands in all the ternary chelates. While, Gly behaves as a monobasic ligand through the carboxylate group. Whereas, PhA behaves as a dibasic ligand through the carboxylate and amino groups. The structure of the ternary chelates is given in Figs. 6 and 7.

References

[1] D.V.R. Rao, J. Ind. Chem. Soc. 71 (1994) 533.
[2] V.V. Ramanujam, U. Krishnan, J. Ind. Chem. Soc. LVII (1980) 359.
[3] L.H. Abdel-Rahman, L.P. Battaglia, M.R. Mohamoud, Polyhedron 15 (1996) 327.
[4] H. Matsui, H. Ohtaki, Bull. Chem. Soc. Jpn. 55 (1982) 461.
[5] J. Maslowska, L. Chruscinski, Polyhedron 3 (1984) 1329.
[6] D.E. Weder, C.T. Dillon, T.W. Hambley, B.J. Kennely, P.A. Lay, J.R. Biffin, H.L. Regtop, N.M. Davies, Coord. Chem. Rev. 232 (2002) 95.
[7] R. Cini, J. Chem. Soc., Dalton Trans. (1996) 111.
[8] D. Di Leo, F. Berrettini, R. Cini, J. Chem. Soc., Dalton Trans. (1998) 1993.
[9] R. Cini, G. Giorgi, A. Cinquantini, C. Rossi, M. Sabat, Inorg. Chem. 29 (1990) 5197.
[10] S.K. Hadjikakou, M.A. Demertzis, J.R. Miller, D. Kolxala-Demertzis, J. Chem. Soc., Dalton Trans. (1999) 663.
[11] A. Bury, A.E. Underhill, D.R. Kemp, N.J. O'Shea, J.P. Smith, P.S. Gomm, Inorg. Chim. Acta 138 (187) 85.
[12] M.R. Moya-Hernandez, A. Mederos, S. Dominguez, A. Orlandini, C.A. Ghilardi, F. Cecconi, E. Gonzalez-Vergara, A. Rojas-Hernandez, J. Inorg. Biochem. 95 (2004) 131.
[13] T. Miyazawa, T. Shimanouchi, S. Mizushima, J. Chem. Phys. 29 (1958) 611.
[14] D.X. West, J.K. Swearingen, J.V. Martinez, S.H. Ortega, A.K. El-Sawaf, F.V. Meurs, A. Castineiras, I. Garcia, E. Bermejo, Polyhedron 18 (1999) 2919.
[15] S.Z. Haider, K.M.A. Malik, J. Bangladesh Acad. Sci. 6 (1982) 119.
[16] E.G. Ferrer, S.B. Etcheverry, E.J. Baran, Monatch. Chem. 124 (1993) 355.
[17] N. Rao, P.V. Rao, V. Raju, M.C. Ganorkar, Indian J. Chem. 24A (1985) 877.
[18] G.K. Sandhu, S.P. Verma, Polyhedron 6 (1987) 587.
[19] A.S.A. Zidan, A.I. El-Said, M.S. El-Meligy, A.A.M. Aly, O.F. Mohamed, J. Therm. Anal. 26 (2000) 665.
[20] P. Largrange, M. Schneider, K. Zare, J. Largrange, Polyhedron 13 (1994) 861.
[21] C.C. Su, T.Y. Tai, S.P. Wu, S.L. Wang, F.L. Liao, Polyhedron 18 (1999) 2361.
[22] G.G. Mohamed, M.A. Zayed, N.E.A. El-Gamel, Spectrochim. Acta 58A (2002) 3167.
[23] J. Kincaidand, K. Nakamoto, Spectrochim. Acta 32A (1976) 277.
[24] F.H. Urena, A.L.P. Chamorro, M.N.M. Carreterro, J.M. Amigo, V. Esteve, T. Debaerdemaeker, Polyhedron 18 (1999) 2205.
[25] A.P. Mishra, S.K. Srivastava, V. Srivastava, J. Indian Chem. Soc. 74 (1997) 487.
[26] M.M. Moustafa, J. Therm. Anal. 50 (1997) 463.
[27] G.G. Mohamed, N.E.A. El-Gamel, F.A.N. El-Dien, Synth. React. Inorg. Met.-Org. Chem. 31 (2001) 347.
[28] A. Hazell, C.J. Mckenzie, L.P. Nielsen, Polyhedron 19 (2000) 1333.
[29] T.J. Hubin, J.M. McCormick, S.R. Collinson, M. Buchalova, C.M. Perkins, N.W. Alcock, P.K. Kahol, A. Raghunathan, D.H. Busch, J. Am. Chem. Soc. 122 (2000) 2512.
[30] F.A. Cotton, G. Wilkinson, C.A. Murillo, M. Bochmann, Advanced Inorganic Chemistry, 6th ed., Wiley, New York, 1999.
[31] M. Velusamy, M. Palaniandavar, K.R.J. Thomas, Polyhedron 17 (1998) 2179.
[32] G.G. Mohamed, Z.H. Abd El-Wahab, J. Therm. Anal. 73 (2003) 347.
[33] N. Mondal, D.K. Dey, S. Mitra, K.M. Abdul Malik, Polyhedron 19 (2000) 2707.
[34] N.R.S. Kumar, M. Nethiji, K.C. Patil, Polyhedron 10 (1991) 365.
[35] P.S. Reddy, K.H. Reddy, Polyhedron 19 (2000) 1687.
[36] J. Sanmartin, M.R. Bermejo, A.M.G. Deibe, M. Maneiro, C. Lage, A.J.C. Filho, Polyhedron 19 (2000) 185.
[37] A.W. Coats, J.P. Redfern, Nature 201 (1961) 68.
[38] C.K. Bhaskare, P.P. Hankare, J. Ind. Chem. Soc. 72 (1995) 585.
[39] A.M. Donia, M.M. Gouda, M.I. Ayad, H.A. El-Boraey, Thermohim. Acta 194 (1992) 155.
[40] Z.M. Zaki, G.G. Mohamed, Spectrochim. Acta 56A (2000) 1245.